Journal of
Water & Climate Change

IWA PUBLISHING

Journal of Water and Climate Change Vol 13 No 10, 3620 doi: 10.2166/wcc.2022.198

Prediction of future groundwater levels under representative concentration pathway scenarios using an inclusive multiple model coupled with artificial neural networks

Mohammad Ehteram[a,*], Zahra Kalantari[b], Carla Sofia Ferreira[c,d], Kwok-Wing Chau[e] and Seyed-Mohammad-KazemEmami[a]

[a] Department of Water Engineering, Semnan University, Semnan, Iran
[b] Department of Sustainable Development, Environmental Science and Engineering, KTH Royal Institute of Technology, SE-10044 Stockholm, Sweden
[c] Department of Physical Geography, Bolin Centre for Climate Research, Stockholm University, SE-10691 Stockholm, Sweden
[d] Research Centre for Natural Resources, Environment and Society (CERNAS), Polytechnic Institute of Coimbra, Coimbra Agrarian Technical School, 3045-601 Coimbra, Portugal
[e] Department of Civil and Environmental Engineering, Hong Kong Polytechnic University, Hong Kong, China
*Corresponding author. E-mail: mohammdehteram@semnan.ac.ir

ABSTRACT

Groundwater (GW) plays a key role in water supply in basins. As global warming and climate change affect groundwater level (GWL), it is important to predict it for planning and managing water resources. This study investigates the GWL of the Yazd-Ardakan Plain basin in Iran for the base period of 1979–2005 and predicts for periods of 2020–2059 and 2060–2099. Lagged temperature and rainfall are used as inputs to hybrid and standalone artificial neural network (ANN) models. In this study, the rat swarm algorithm (RSA), particle swarm optimisation (PSO), salp swarm algorithm (SSA), and genetic algorithm (GA) are used to adjust ANN models. The outcomes of these models are then entered into an inclusive multiple model (IMM) as an ensemble model. In this study, the output of climate models is also inserted into the IMM model to improve the estimation accuracy of temperature, rainfall, and GWL. The monthly average temperature for the base period is 12.9 °C, while average temperatures for 2020–2059 under RCP 4.5 and RCP 8.5 scenarios are 14.5 and 15.1 °C, and for 2060–2099 they are 16.41 and 18.5 °C under the same scenarios, respectively. In future periods, rainfall is low in comparison with the base period. Lagged rainfall and temperature of the base period are inserted into ANN-RSA, ANN-SSA, ANN-PSO, ANN-GA, and ANN models to predict GWL for the base period. Outputs of IMM, ANN, and the five hybrid models (ANN-RSA, ANN-SSA, ANN-PSO, and ANN-GA) indicate that root mean square errors (RMSE) are 2.12, 3.2, 4.58, 6.12, 6.98, and 7.89 m, respectively, in the testing level. It is found that GWL depletion in 2020–2059 under RCP 4.5 and RCP 8.5 scenarios are 0.60–0.88 m and 0.80–1.16 m, and in 2060–2099 under the same scenarios they are 1.49–1.97 m and 1.75–1.98 m, respectively. The results highlight the need to prevent overexploitation of GW in the Ardakan-Yazd Plain to avoid water shortages in the future.

Key words: climate models, RCP scenarios, soft computing models, sustainable water resource management

HIGHLIGHTS

- Introducing a new ensemble model for integrating outputs of general circulation models.
- Introducing a new ensemble model for predicting GWL.
- Introducing a new feature selection method for choosing the best inputs.

GRAPHICAL ABSTRACT

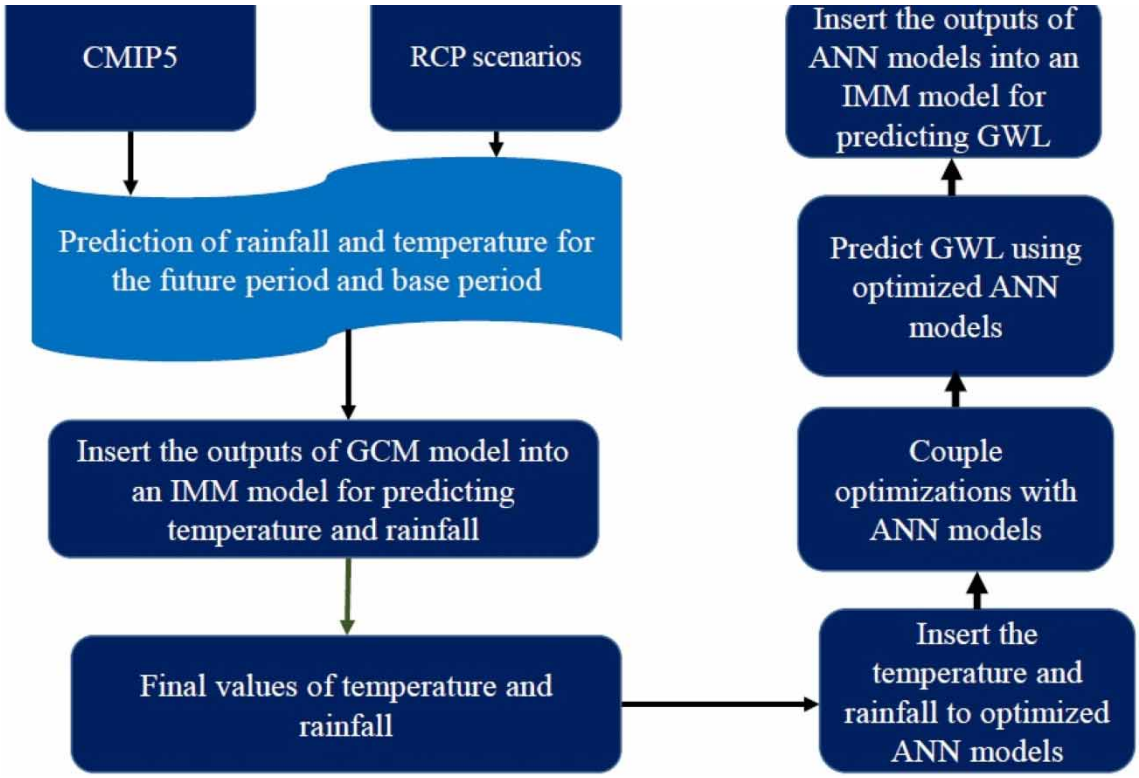

1. INTRODUCTION

Population growth, droughts, and water scarcity are challenges faced by decision-makers in terms of water supply (Farrokhi *et al.* 2021; Ghanbari-Adivi *et al.* 2022). Groundwater (GW) is an important global water supply source subject to increasing overexploitation. Predicting variations in the groundwater levels (GWL) driven by climate change is an important topic to ensure water supply and appropriate management at basin scale for future scenarios (Banadkooki *et al.* 2020). Sustainable water resource management is an important topic for managers (Chitsazan *et al.* 2015; Ghazi *et al.* 2021; Gong *et al.* 2018; Gong *et al.* 2016; Rezaie-balf *et al.* 2017; Yoon *et al.* 2016). Tapoglou *et al.* (2014) conducted a study to investigate the effects of different climate scenarios on the GWL of a basin in Greece and concluded that decreasing precipitation will reduce the basin's GWL. Shrestha *et al.* (2016) used MODFLOW and combined model intercomparison project phase 5 (CMIP5) to predict GWL in future periods for a basin in Vietnam. They reported that the temperature would increase by 1.5 and 4.9 °C by the end of the 21st century under representative concentration pathway (RCP) 4.5 and 8.5, respectively, and that GWL would drop in short, medium, and long-terms. Chang *et al.* (2016) reported that under climate change, some aquifers in the USA might not supply the required water for future periods. Zhou *et al.* (2020) also showed the impact of climate change on the GW flow dynamics in China and the changing pattern in GWL. Patil *et al.* (2020) showed that temperature and rainfall increase by 2.59 °C and 81.50%, respectively, expected for the period 2021–2050, will lead to a GW recharge increase of 24.91% in the Hiranyakeshi watershed. Based on general circulation models and the MODFLOW model, Shrestha *et al.* (2020) also predicted a future GWL decline in Nepal. Based on Hamidov *et al.* (2020), climate change is expected to decrease GWL from 1.75 m in 2050 to 1.79 m by 2100 in north-west Uzbekistan. In the lake Tana basin, in Ethiopia, Tigabu *et al.* (2021) predicted surface runoff increases and the GWL declines under RCP 4.5 and RCP 8.5 scenarios.

An investigation of the effects of climate change on GWL involves multiple steps (Figure 1(a)). Modellers have introduced different models to predict GWL, such as numerical models and machine-learning models (Huang *et al.* 2017; Natarajan & Sudheer 2020). Numerical models require the establishment of boundary conditions, involve complex equations, and some can require many inputs, which makes them time-consuming when predicting the GWL. In recent years, machine-learning models have been widely utilised to predict GWL of different basins (Table 1A, Appendix A). The advantages of machine-learning

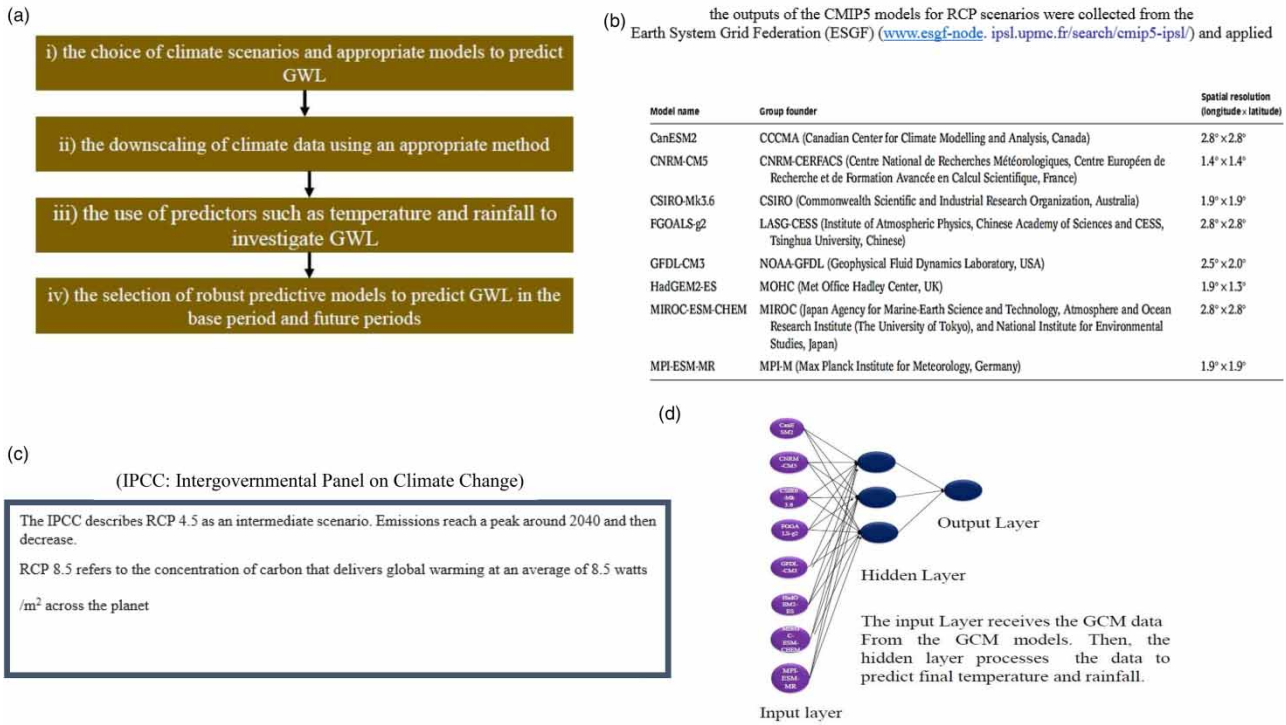

Figure 1 | (a) The levels of modelling process for predicting GWL, (b) name of GCMs included in CMIP5, (c) definition of RCP scenarios investigated, (d) structure of the ensemble model using outputs of CMIP5 models to predict temperature and rainfall (circles shows neurons of each layer).

algorithms are their precise and fast convergence, and high flexibility (Ehteram *et al.* 2021a, 2022). Although individual models are robust tools for prediction purposes, ensemble models based on the use of data from multiple individual models can reduce computational errors in the modelling process (Ehteram *et al.* 2021b). However, a few studies have used ensemble models to predict GWL (Yin *et al.* 2021).

The main aim of this paper is to predict monthly GWL for future medium- (2020–2059) and long-term periods (2060–2099) based on rainfall and temperature from a base period (1979–2005) in one of Iran's key basins. Future GWL is based on climate change conditions based on CMIP5 using RCP 4.5 and RCP 8.5 scenarios. The study addresses the following research gaps related to the prediction of GWL:

1. Individual climate models may not give accurate outputs. In this study, an ensemble framework is suggested to provide temperature and rainfall data based on individual climate models (Sharafati *et al.* 2020a). Temperature and rainfall data are provided based on climate models under RCP scenarios, using downscaling methods and outputs are then inserted into an ANN model as an ensemble model. The temperature and rainfall outputs of the ensemble models are the weighted outputs of the climate models.

   Although ANN models have great potential for predicting GWL (Table 1A), robust optimisation algorithms should be used to adjust ANN parameters. In this paper, a new evolutionary algorithm, the rat swarm algorithm (RSA), is applied to train ANN models. RSA is easy to implement and is a robust optimisation algorithm for finding an accurate solution (Dhiman *et al.* 2021). To assess RSA's ability to train ANN, RSA is benchmarked against multiple optimisation algorithms (Dhiman *et al.* 2021). Even though there are tools like deep learning for simulation, their modelling process is complex. Preparing structures and parameters for deep learning models may be complex and time-consuming. Thus, hybrid and optimised ANN models are robust and reliable for predicting variables.
2. While previous studies only used individual ANN models for predicting GWL, this study introduces an ensemble model, namely the inclusive multiple model (IMM)-ANN, to predict GWL. The IMM-ANN uses outputs of ANN-PSO, ANN-RSA

and ANN-GA to achieve the final outputs of GWL. The IMM model reduces computational errors during the modelling process.

3. One of the research gaps identified in previous studies is the lack of a proposal for a global strategy to determine inputs. In this article, lagged temperature and rainfall data are utilised as inputs to the models for predicting GWL. To determine the time lags of inputs, a new test, namely the hybrid gamma test-RSA (GT-RSA), is used in this study.

A key objective of this project is to predict GWL under climate change conditions. Modelling GL under climate change is challenging. Modellers need GCM outputs to predict temperature and rainfall. Incorporating the outputs of GCM models into an ensemble model can improve accuracy. Next, we need to predict GWL. Because the GWL depends on different factors, robust models are needed. Our study introduces a new ensemble for predicting GWL under climate change. Using the outputs of the GCM model, the new ensemble model predicts temperature and rainfall. Unlike other ensemble models, the new model does not require complicated computations. As an example, the Bayesian model averaging requires prior and posterior distributions. Furthermore, the paper introduces a new method for selecting inputs based on climate parameters. Modellers can use this method when they have a large number of inputs. In the final step, we build new MLP models for predicting the GWL and climate parameters using new optimisation algorithms. Our paper presents a new ensemble model, a new hybrid GT, and new MLP models for predicting GWL and climate parameters.

2. MATERIAL AND METHODS

2.1. Outline of the current study

The outline of the current study is as follows:

1. As a first step, rainfall, temperature, and GWL data were collected for the base period (1979–2005). The RCP 4.5 and 8.5 scenarios from CMIP5 models were used to simulate temperature and rainfall for future medium- (2020–2059) and long-term periods (2060–2099). As the outputs of the models are large scale, we downscaled them (see section 2.2) to provide more reliable estimations. While it may be possible to obtain high-resolution downscaled datasets, this study used large-scale GCM outputs to illustrate the application of downscaling methods for downscaling data.
2. The downscaled data of GCM models, i.e. temperature and rainfall, were inserted into an ANN model as an IMM model to improve accuracy. Using the IMM model and individual GCM models, the best model for predicting future temperature and rainfall is determined. The IMM models are explained in section 2.3.7.
3. RSA is coupled with the GT to choose the best inputs and reduce the complexity of gamma tests. Section 3.1 presents the structure of the hybrid GT. This test is used to determine the best input data for predicting targets.
4. Optimisation algorithms are coupled with ANN models to create optimised ANN models.
5. ANN-RSA, ANN-SSA, ANN-PSO, ANN-GA, ANN-ANN, and ANN models are used to predict GWL, temperature, and rainfall (outputs).
6. For the future and base period, the outputs of hybrid individual ANN models were inserted into the IMM model.
7. Finally, the status of GWL for the future and base period is examined.

2.2. Climate models and scenarios

In this study, two RCP scenarios, namely RCP 4.5 and RCP 8.5, are used, along with multiple climate models (CMIP5), summarised in Figure 1(b). The definition of RCP scenarios is given in Figure 1(c). Figure 1(d) shows the structure of IMM as an ensemble model for predicting temperature and rainfall. Decision-makers requested climate models (CMIP5) and RCP scenarios for water resource planning and management. CMIP6 models can be used for simulations in future studies. In this study, the CMIP5 models were used. In the next studies the results of the CMPIP5 and CMPI6 models will be compared.

The large scale of the computational grid in terms of time and space leads to computational errors, thus downscaling of outputs of climate models is an important task for modellers. There are different methods for downscaling the outputs of CMIP5 models (e.g. statistical and dynamic) as shown in Figure 1(a). In this study, simple methods, namely proportional and change factor approaches, are used to downscale the outputs of CMIP5 models spatially and temporally. To spatially downscale outputs of CMIP5 models, information from GCMs for a primary grid box containing the study area is obtained. This method is called the proportional method. The difference (or ratio) between the average of a CMIP5 model's dataset for

the future and the corresponding average of CMIP5 models simulated for the base period is computed to temporally downscale outputs of CMIP5 models. This is known as the change factor (Ashofteh *et al.* 2015). Downscaled rainfall and temperature data are obtained as follows (Ashofteh *et al.* 2015):

$$\Delta Te_i = (\bar{T}_{GCM,fut,i} - \bar{T}_{GCM,base,i}) \tag{1}$$

$$\Delta R_i = \left(\frac{\bar{R}_{GCM,fut,i}}{\bar{R}_{GCM,base,i}}\right) \tag{2}$$

where ΔTe_i and ΔR_i are the changes in average temperature and rainfall for a month i, $\bar{R}_{GCM,fut,i}$ and $\bar{R}_{GCM,base,i}$ are the average long-term monthly rainfall for a month i in future and base periods simulated by CMIP5 models, respectively, and $\bar{T}_{GCM,fut,i}$ and $\bar{T}_{GCM,base,i}$ are the average long-term monthly temperature for month i in future and base periods, respectively. Finally, temperature and rainfall for future periods are computed as follows:

$$Te_i = Te_{\mathrm{obs},i} + \Delta T_i \tag{3}$$

$$R_i = R_{\mathrm{obs},i} + \Delta R_i \tag{4}$$

where $Te_{\mathrm{obs},i}$ is the observed temperature, $R_{obs,i}$ is the observed rainfall, R_i is rainfall for the future period, and Te_i is the temperature for the future period. Equations (3) and (4) give downscaled climate data. To increase the accuracy of outputs, the IMM model is used as an ensemble model. When CMIP5 models give downscaled temperature and rainfall, each of the outputs is inserted into the ANN model. This process, which helps improve the accuracy of outputs, is shown in Figure 1(c). In the next section, the theory and structures of IMM, optimisation algorithms, and ANN are explained.

2.3. Machine-learning models used to predict GWL

2.3.1. Structure of ANN models

Because of its ease of implementation, flexibility, and reliability, the ANN model is chosen. An ANN model mimics the behaviour of the brain and consists of different layers. Predictors are received by the first layer, which is known as the input layer. Middle layers process the information received from the input layer and use activation functions to provide relationships between inputs and outputs (Ehteram *et al.* 2021a; Lee *et al.* 2019). The activation function of middle layers, using input values and weight connections between the first layer and middle layers, provides outputs that are inserted as inputs into the output layer (Seifi *et al.* 2022). The activation function of the last layer gives the final outputs (Ehteram *et al.* 2021b). Figure 2(a) shows a typical mathematical model of ANN. In the structure of ANN, the bias as a constant term and weight connections are two important parameters. Although methods such as gradient descent can be applied to adjust ANN parameters, they are unreliable (Ehteram *et al.* 2021a). Optimisation algorithms are robust tools for adjusting ANN parameters (Ehteram *et al.* 2021b). Multiple optimisation algorithms are used to adjust the weights and biases in this study. Figure 2(b) outlines the structure of ANN.

Modellers need fast calculation and convergence when training ANNs. A high degree of accuracy and fast computation are two main reasons for applying different optimisation algorithms (Mohanty *et al.* 2015). Ideally, algorithms should have fewer random parameters. PSO, RSA, SSA, and GA were chosen for this study due to their high accuracy, fast convergence, and good balance between exploration and exploitation. In addition, the algorithms are easy to develop. Two parameters of RSA are unknown: the size of the population and the number of iterations. Therefore, RSA does not have many unknown parameters. The modelling uncertainty decreases when the algorithm does not have many random parameters. SSA leaders guide the other solutions towards optimal solutions. As a result, SSA can find the best solutions earlier.

2.3.2. Rat swarm algorithm

Dhiman *et al.* (2021) introduced RSA based on the life of rats. The advantages of RSA are the low number of computational levels, easy implementation, and high accuracy. In the first step, an initial location is defined for each rat. The best rat is

(a)

$$Y_k = f_0\left[\sum_{i=1}^{M_N} W_{kj} \times f_h\left(\sum_{i=1}^{N_N} W_{ji} X_i + b_{jo}\right) + b_{ko}\right]$$

f_o: The activation function of output, f_h: The activation function of hidden layer, X_i: The input variable, W_{ij}:a weight in the hidden layer connecting the ith neuron in the input layer and the jth neuron in the hidden layer, W_{kj}: a weight in the output layer connecting the jth neuron in the hidden layer and the kth neuron in the output layer b_{jo}:the bias for the jth hidden neuron, b_{ko}: the bias for the kth output neuron, N_N: The Number of inputs, and M_N: The number of hidden neurons.

(b)

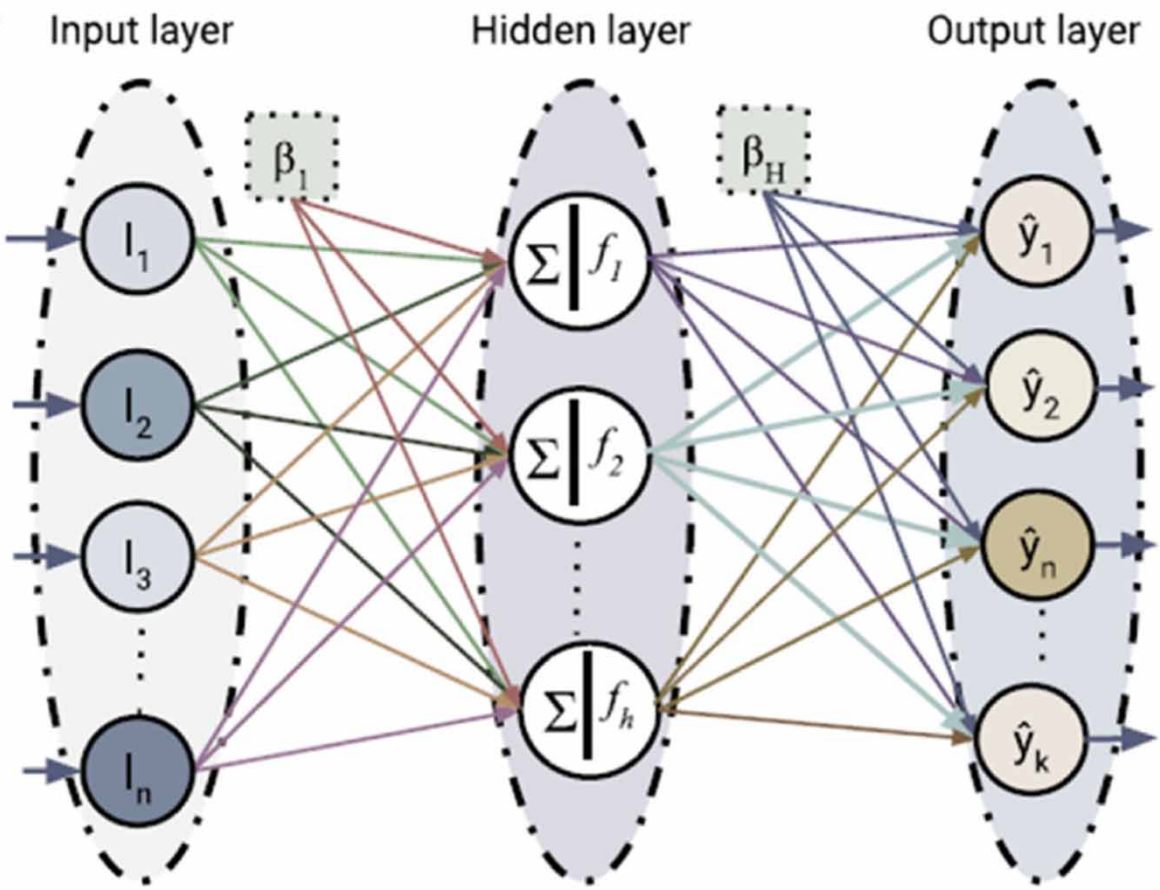

Figure 2 | (a) Mathematical model of ANN, (b) structure of ANN model (I: input, f: activation function, output, and β: bias) (Jalali *et al.* 2020).

determined by the computation of a fitness function. Rats then change their positions:

$$\vec{RA} = A.\vec{RA}_i(x) + \chi.(RA_r - \vec{RA}_i(x)) \tag{5}$$

where $\vec{RA}_i(x)$ is the location of rats, RA_r is the location of the best rat, χ and A are the control parameters, and $\vec{RA}$ is the new locations of rats. Then A and χ are computed as follows:

$$A = ra - it \times \frac{ra}{it_{\max}} \tag{6}$$

$$\chi = 2.rand \tag{7}$$

where ra is a random number, it is the number of iterations, $it_{\max}$ is the maximum number of iterations, and $rand$ are random numbers. In the next level, the behaviour of fighting prey is simulated as follows:

$$\vec{RA}_i(x+1) = |\vec{RA}_r(x) - \vec{RA}| \tag{8}$$

where $\vec{RA}_i(x+1)$ is the new location of rats after fighting with prey. Equation (8) determines the final locations of rats. Figure 3 shows the RSA flowchart for solving optimisation problems.

2.3.3. Salpswarm algorithm

The salpswarm algorithm (SSA), which was introduced by Mirjalili *et al.* (2017), is a robust optimisation algorithm and mimics the life of salps. The advantages of SSA are its fast convergence, advanced operators for escaping from local optimums, and high accuracy. Salps have a social life. A salp with the best objective function guides others. The location of

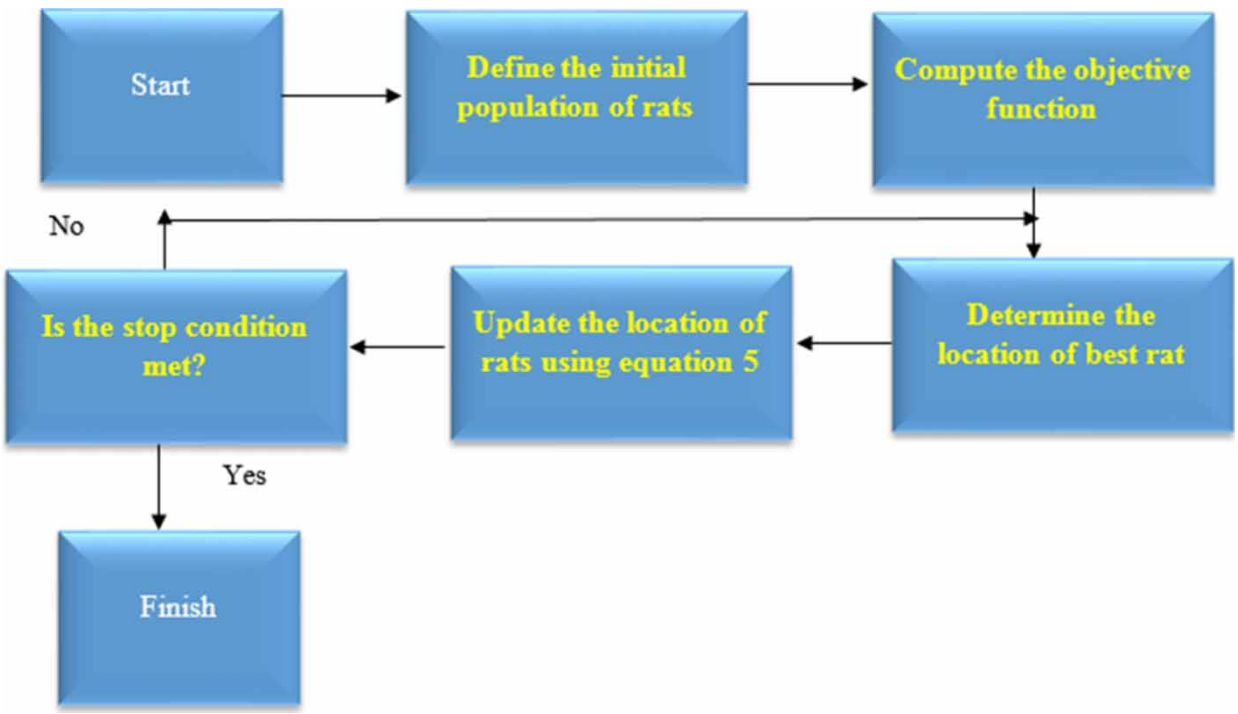

Figure 3 | RSA flowchart for solving optimisation problems.

the best salp as a leader is as follows:

$$la_j^1 = \begin{bmatrix} FO_j + \alpha_1((up_j - lo_j)\alpha_2) + lo_j, \alpha_3 \geq 0 \\ FO_j - \alpha_1((up_j - lo_j)\alpha_2) + lo_j, \alpha_3 < 0 \end{bmatrix} \tag{9}$$

where la_j^1 is the location of the best salp, FO_j is the location of food (the best solution), lo_j and up_j are the lower and upper bounds of decision variables, respectively, and α_3, α_1, α_2 are random variables. In the next phase, the locations of followers are obtained as follows:

$$sa_j^i = \frac{1}{2}(sa_j^i + sa_j^{i-1}) \tag{10}$$

where sa_j^i is the location of the ith follower in the jth dimension, and sa_j^{i-1} is the location of the $(i-1)$th follower in the jth dimension. Figure 4 shows the Salp flowchart for solving optimisation problems.

2.3.4. Particle swarm optimisation

Different optimisation problems can be solved by particle swarm optimisation (PSO). Advantages of PSO are its easy implementation and high accuracy (Ehteram *et al.* 2021b). For each particle, components of velocity and position are first determined and then the fitness function is computed for each particle. Each particle updates its location and velocity (Ehteram *et al.* 2021b):

$$VE_{ij}^{t+1} = \omega VE_{i,j}^t + v_1 ra_1(PO_{ij}^{p(t)} - PO_{ij}^{(t)}) + v_2 ra_2(PO_{ij}^{g(t)} - PO_{ij}^{(t)}) \tag{11}$$

$$PO_{ij}^{t+1} = PO_{ij}^t + VE_{ij}^{t+1} \tag{12}$$

where VE_{ij}^{t+1} is the velocity of the ith particle in the jth dimension at iteration $t+1$, $VE_{i,j}^t$ is the velocity of the ith particle in the jth dimension at iteration, v_1 and v_2 are acceleration coefficients, ra_2 and ra_1 are random numbers, $PO_{ij}^{p(t)}$ is the local best

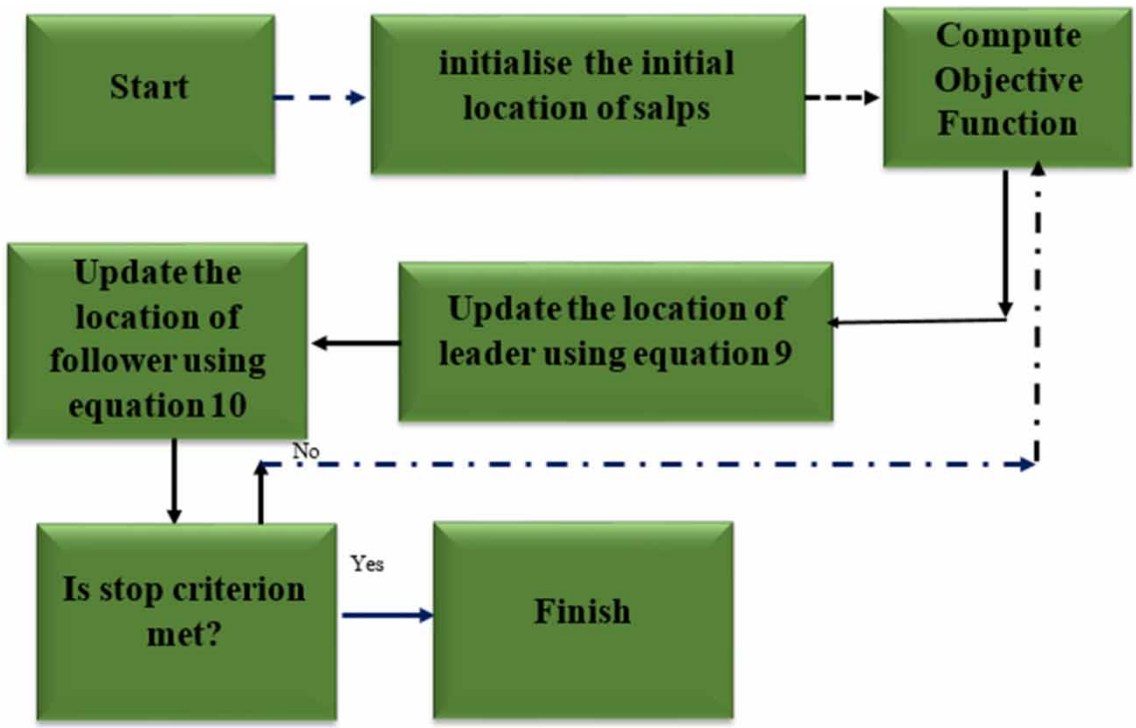

Figure 4 | Salp flowchart for solving optimisation problems.

location, $PO_{ij}^{g(t)}$ is the global best location, and PO_{ij}^{t+1} and PO_{ij}^{t} are the positions of the ith particle in the jth dimension at iterations $t+1$, and t, respectively. The optimisation process stops when the stop criterion is met. When the locations of particles are updated, the values of decision variables in an optimisation problem are updated.

2.3.5. Genetic algorithm

In optimisation, genetic algorithm (GA) is known as a useful evolutionary algorithm. GA, based on three operators, namely mutation, crossover, and selection, provides high-quality solutions (Li *et al.* 2021). The use of mutation operators increases the diversity of solutions. For this reason, GA can have a high ability to solve complex problems (Abdullah *et al.* 2021). Chromosomes are agents of GA and the quality of each chromosome is determined by computing the fitness function. Afterwards, different operators of GA are used to update the solutions (Li *et al.* 2021). A selection operator is applied to identify the best chromosomes with the best values of the objective function. In GA, crossover is utilised to combine the genetic information of two parents to generate a new offspring. To maintain the diversity of chromosomes, a mutation operator is used. In a mutation, a gene on the chromosomes is randomly changed. The optimisation process finishes when the stop condition is met. However, the optimisation algorithms are reliable tools for adjusting ANN parameters. The next section explains the structure of hybrid ANN models using optimisation algorithms.

2.3.6. Hybrid optimisation algorithms and ANN models

In this research, the ANN parameters are defined as decision variables of optimisation algorithms. The ANN parameters are obtained using optimisation algorithms as follows:

1. ANN models are applied to estimate the data in the training phase.
2. If the stop condition is satisfied, testing data is used to run ANN models in the testing phase, otherwise ANN models go to the next phase.
3. Parameters of ANN models, including weight and bias, are considered as the initial population of optimisation algorithms.
4. The precision of ANN models is determined by the computation of fitness functions. In this study, root mean square error (RMSE) is utilised as the fitness function. For each set of parameters, the ANN model run is computed using training data and the objective function.
5. Operators of different optimisation algorithms are applied to update the positions of agents, which represent values of decision variables. Thus, changes in positions of agents in an optimisation algorithm mean updates of ANN parameters.
6. The stop condition is monitored. If it is satisfied, the algorithms go to stage 3 and the model moves to the next phase; otherwise the model moves to stage 5.

2.3.7. Inclusive multiple models

Standalone and hybrid ANN models are considered as individual models. The outputs of multiple individual models can be embedded into the structure of an ensemble model, and then this ensemble model can be used to prepare the final outputs (Abbaszadeh *et al.* 2021). Indeed, the IMM model receives outputs from multiple individual models as inputs. Then, the IMM model predicts target variables based on received inputs (Abbaszadeh *et al.* 2021). In this study, the IMM model is used to assemble climate models and ANN models. First, the ANN model, as an IMM model, receives outputs from CMIP5 for predicting rainfall and temperature. In the second section, the ANN model, as the IMM model, receives outputs from ANN-RSA, ANN-SA, ANN-GA, ANN-PSO, and ANN models for predicting GWL. Figure 5 illustrates the structure of the IMM model.

2.4. Data analysis

Several error indices are utilised for determining the precision of models. Different indicators are used to evaluate the models comprehensively. We can identify the best model using these indicators.

1. root mean square error (RMSE)

$$\mathrm{RMSE}\sqrt{\frac{\sum_{i=1}^{N}(\mathrm{GWL}_{\mathrm{ob}}-\mathrm{GWL}_{\mathrm{es}})^2}{N}} \tag{13}$$

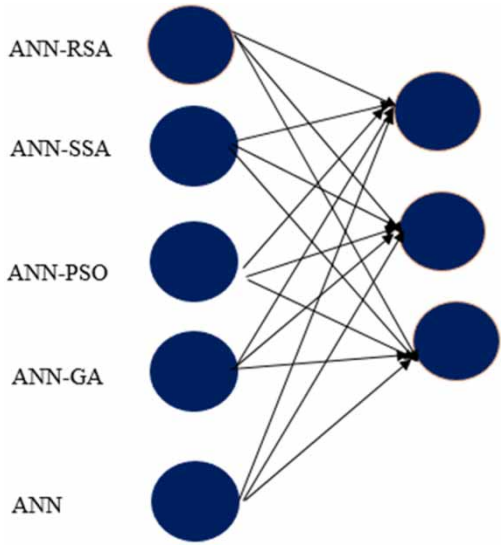

Figure 5 | Structure of the IMM model.

2. mean absolute error (MAE)

$$\mathrm{MAE} = \frac{\sum_{i=1}^{M} |\mathrm{GWL_{ob}} - \mathrm{GWL_{es}}|}{n} \tag{14}$$

3. Nash-Sutcliffe efficiency (NSE)

$$\mathrm{NSE} = 1 - \frac{\sum_{i=1}^{n} (\mathrm{GWL_{ob}} - \mathrm{GW_{es}})^2}{\sum_{i=1}^{n} (\mathrm{GW_{ob}} - \bar{\mathrm{GW}}_{\mathrm{ob}})^2} \tag{15}$$

4. percentage of bias (PBIAS)

$$\mathrm{PBIAS} = \frac{\sum_{i=1}^{n} (\mathrm{GWL_{obs}} - \mathrm{GWL_{es}})}{\sum_{i=1}^{n} (Q_{\mathrm{obs}})} \tag{16}$$

where $\mathrm{GWL_{es}}$ is estimated GWL, $\mathrm{GWL_{ob}}$ is observed GWL, N is a number of data, $\bar{\mathrm{GWL}}_{\mathrm{es}}$ is an average estimated GWL and $\bar{\mathrm{GWL}}_{\mathrm{ob}}$ is an average observed GWL.

The accuracy of a model cannot be evaluated with a single error index. Different indices were used to determine the best model for predicting temperature, rainfall, and GWL. Using different error indices, the best model should be superior to the others. Different characteristics of each error index aid modellers in making better judgments.

3. CASE STUDY

The Yazd-Ardakan Plain is one of the most important basins in central Iran (Figure 6(a)) covering an area of 2,491 km^2. The climate of the basin is arid. The average monthly temperature and rainfall are 20.2 °C and 12.3 mm, respectively (Figure 6(b) and 6(c)). In recent decades, over 800 medium-deep and deep wells in different regions have been excavated for GW abstraction. An average annual drop of 80 cm in GWL of the basin has been observed (Figure 6(d)). GW in this basin is used to meet

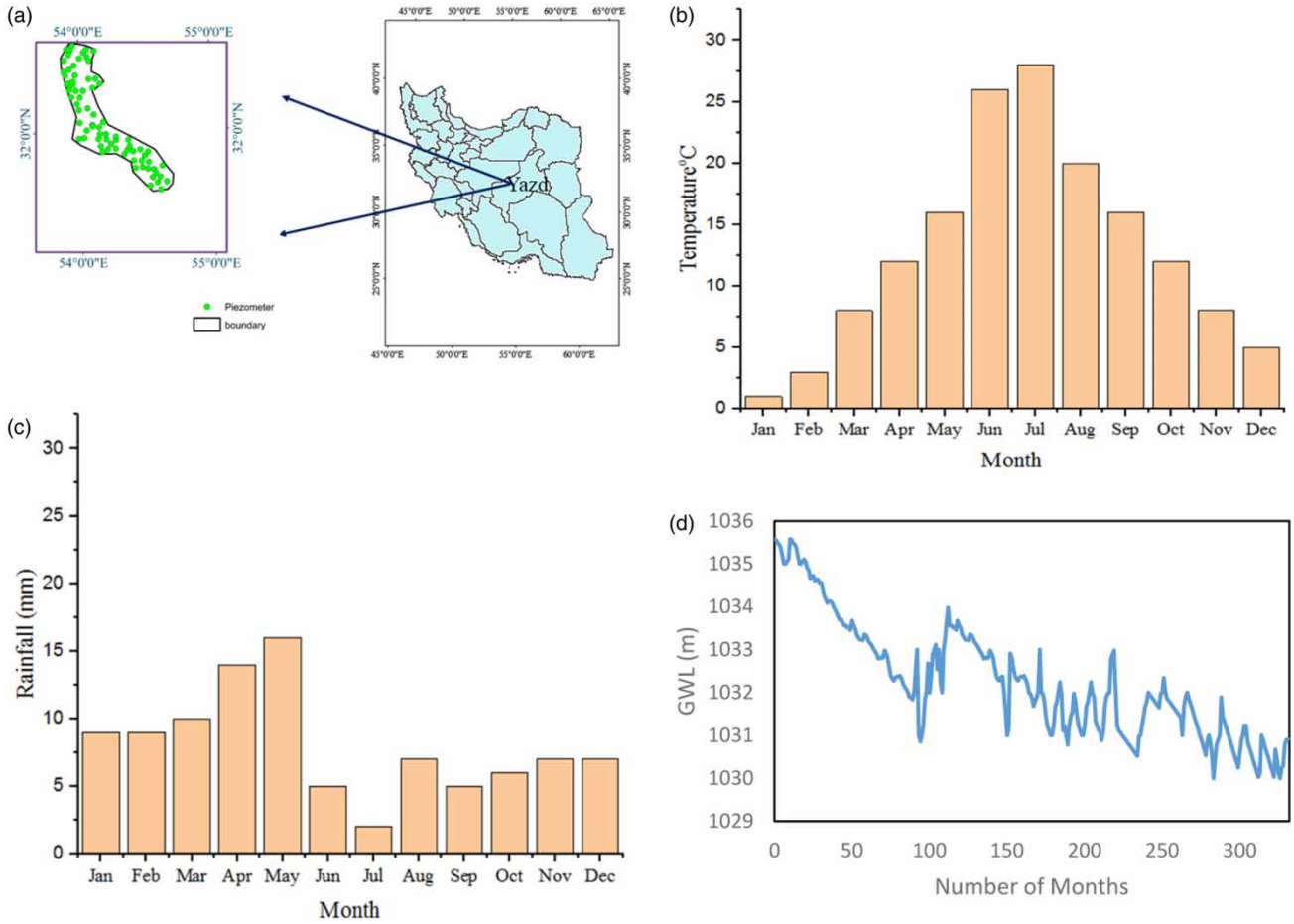

Figure 6 | (a) Location of the case study, (b) average monthly temperature for the base period (1979–2005), (c) average monthly rainfall for the base period, and (d) GWL time series over the base period.

demands for agriculture and irrigation, making its GWL an important issue for decision-makers. The decrease in rainfall and successive droughts in the basin have also increased the complexities of decision-making for water supply. Aridity and drought are the main problems in Yazd. Iran's Yazd-Ardakan desert is one of the largest deserts in Iran. The confined aquifer is observed in the Yazd-Ardekan. Different regions of the Yazd-Ardakan desert experience different rates of water level drop. Generally, there is a maximum and minimum GWL in January and July, respectively. The northeastern areas of the desert have the lowest water levels. Because of the dry climate in the area and a large number of consumers, predicting the aquifer level is highly important. Water quality is good in the west, southwest, and south. The west region of the plain has the highest discharge for drinking water.

3.1. Gamma test

In this study, lagged rainfall and temperature data are utilised as inputs to the models. To determine the best input scenario, the GT is used in this study. GT has been used in different fields, such as sediment modelling (Malik *et al.* 2019), estimation of evapotranspiration (Seifi& Riahi 2020), rainfall runoff modelling (Singh *et al.* 2018), and pan evaporation modelling (Malik *et al.* 2020). A dataset is assumed to be as follows (Noori *et al.* 2011):

$$\{[in_1 \ldots, in_m(i), out_i]\} = \{(in_i, out_i) | 1 \leq i \leq M\} \tag{17}$$

where in_m is the mth input, M is the number of patterns, m is the number of input parameters, and out_i is the output variable.

In the next phase, delta and gamma functions are computed as follows:

$$\delta_m(k) = \frac{1}{M}\sum_{i=1}^{M} |in_{[N,k]} - in_i|^2,\ k \le 1 \le p \tag{18}$$

$$\gamma_m(k) = \frac{1}{2M}\sum_{i=1}^{M} |out_{[N,k]} - out_i|^2,\ (1 \le k \le p) \tag{19}$$

where $\delta_m(k)$ is the delta function, $\gamma_m(k)$ is the gamma function, $in_{[N,k]}$ is the kth nearest neighbour for each input vector, and $out_{[N,k]}$ is the corresponding out_i-value for the kth nearest neighbour. Gamma uses two important indices, namely V_{ratio} and Γ, for determining the best input scenario:

$$\gamma = A\delta + \Gamma \tag{20}$$

where A is the slope of the line, and

$$V_{\text{ratio}} = \frac{\Gamma}{\sigma^2(out)} \tag{21}$$

where $\sigma^2(out)$ is the variance of outputs. The best input combination gives the smallest values of Γ and V_{ratio}. In this study, rainfall and temperature with lag times of $(t-1)$ to $(t-12)$ are used as inputs to models, giving 2^{24}–1 input scenarios. If the original version of the GT is used, it would be difficult to compute Γ and V_{ratio} for 2^{24}–1 input scenarios. Thus, GT is integrated with RSA for this purpose. First, names of input variables are inserted into RSA as the initial population. A random population is provided using different input variables. The initial population based on input variables includes different input combinations. Afterwards, Γ is computed as an objective function. In the next phase, operators of RSA will be used to update solutions. In RSA, the location of rats represents an input combination including different input variables. When the location of rats is updated, the new input combination is provided. The optimisation process continues until the lowest Γ is provided. A hybrid GT is illustrated in Figure 7, which includes input variable names. The input variables are introduced as the algorithm's initial population. Agents' locations are updated and new input combinations are provided using algorithm operators.

4. RESULTS AND DISCUSSION

4.1. Temperature and rainfall prediction

Figure 8(a) investigates the precision of CMIP5 models and IMM for predicting temperature in the base period. IMM has the lowest RMSE, MAE and PBIAS among all models. RMSEs of IMM, CanESM2, CNRM-CM5, CSIR0-Mk 3.6, FOGALS-g2, GFDL-CM3, HadGEM2-ES, MIROC-ESM-CHEM and MPI-ESM-MR are 0.87, 1.2, 1.34, 1.18, 1.15, 1.12, 1.1, 1.06 and 0.98, respectively. NSE, PBIAS, and MAE of IMM for predicting temperature in the base period are 0.97, 5%, and 0.65 °C, respectively. Figure 8(b) compares the performance of CMIP5 and IMM models for predicting rainfall in the base period. It shows that MAEs of IMM, CanESM2, CNRM-CM5, CSIR0-Mk 3.6, FOGALS-g2, GFDL-CM3, HadGEM2-ES, MIROC-ESM-CHEM, and MPI-ESM-MR are 0.71, 1.14, 1.28, 1.12, 1.10, 1.07, 1.05, 1.01, and 0.93 mm, respectively. NSEs of IMM, CanESM2, CNRM-CM5, CSIR0-Mk 3.6, FOGALS-g2, GFDL-CM3, HadGEM2-ES, MIROC-ESM-CHEM, and MPI-ESM-MR are 0.94, 0.83, 0.81, 0.80, 0.84, 0.86, 0.90, 0.91, and 0.92, respectively, for predicting rainfall. IMM provides the greatest accuracy in predicting rainfall because it takes advantage of multiple climate models. In the next phase, outputs of models under RCP 4.5 and RCP 8.5 are prepared for future periods.

Figure 9 shows values of rainfall and temperature for future periods based on the outputs of IMM using RCP 4.5 and RCP 8.5. The monthly average temperature for the base period is 12.9 °C, while average temperatures for 2020–2099 and 2060–2099 periods under the RCP 4.5 scenario are 14.5 and 16.41 °C, respectively (Figure 9(a)). Monthly average temperatures for 2020–2059 and 2060–2099 under RCP 8.5 are 15.1 and 18.5 °C, respectively. Results reveal that temperatures in future periods under RCP scenarios are higher than in the base period. Figure 9(b) shows monthly average rainfall for future periods under RCP 4.5 and RCP 8.5. The monthly average rainfall for the base period is 7.33 mm, while average rainfall for the 2020–

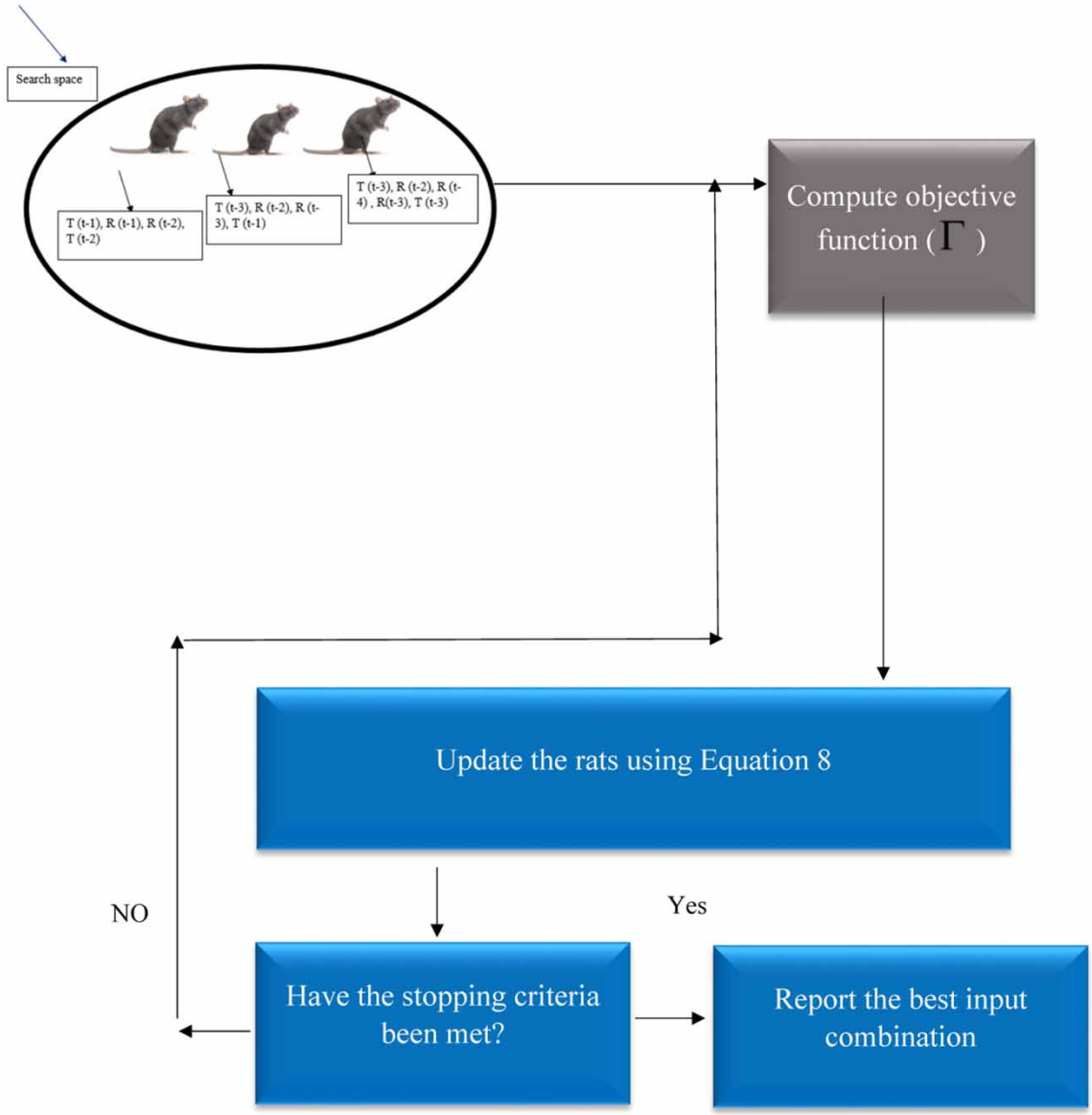

Figure 7 | The structure of the hybrid GT.

2099 and 2060–2099 periods under the RCP 4.5 scenario is 5.91 mm and 4.25 mm, respectively. Average rainfalls under RCP 8.5 for the 2020–2099 and 2060–2099 periods are 5.25 mm and 3.41 mm, respectively. Results indicate that future rainfall will be lower than in the base period. RCP 8.5 provides higher temperatures and lower rainfall than RCP 4.5.

4.2. Selection of inputs

In this study, temperature and rainfall are used as inputs to predict monthly GWL. Lagged rainfall and temperature are chosen by a hybrid GT test. Table 1 shows the first to third best input combinations. The best input combination includes TE($t-1$), TE ($t-2$), RA ($t-1$), RA ($t-2$), RA ($t-3$). It is obtained automatically, therefore modellers do not have to test many input combinations. A correlation test can determine significant input parameters but does not give the best input scenario.

To verify the performance of GT-RSA, heat map correlation is used to determine significant inputs. Figure 10 indicates that T ($t-1$), T ($t-2$), R ($t-3$), R ($t-1$) and R ($t-2$) have the highest correlation with GWL. The best input combination also includes these variables. Thus, GT-RSA correctly determines significant inputs for the best input combination. An increased

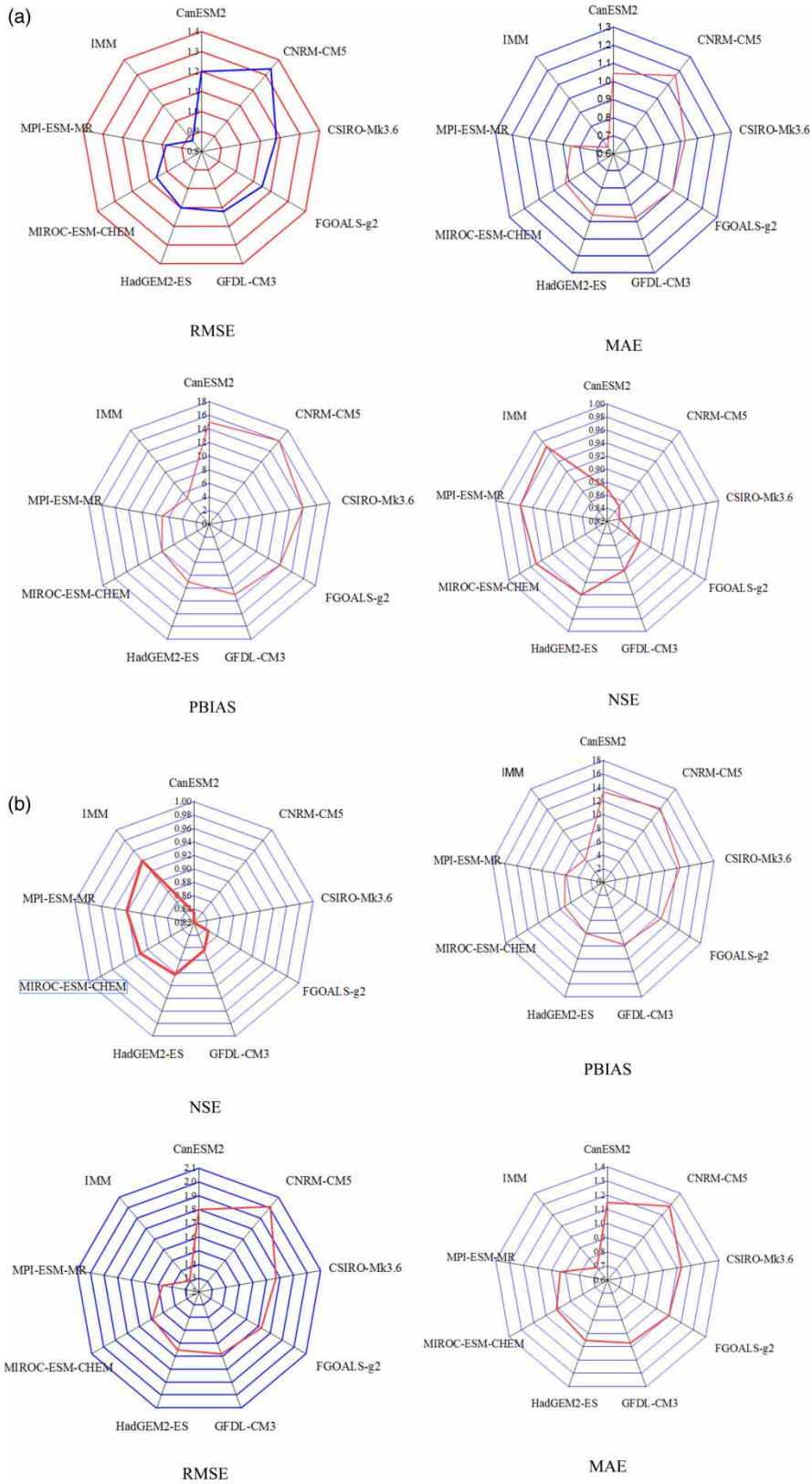

Figure 8 | Comparison of climate models for predicting temperature (a) and rainfall (b) for the base period (1979–2005), based on RMSE, MAE, NSE, and PBIAS.

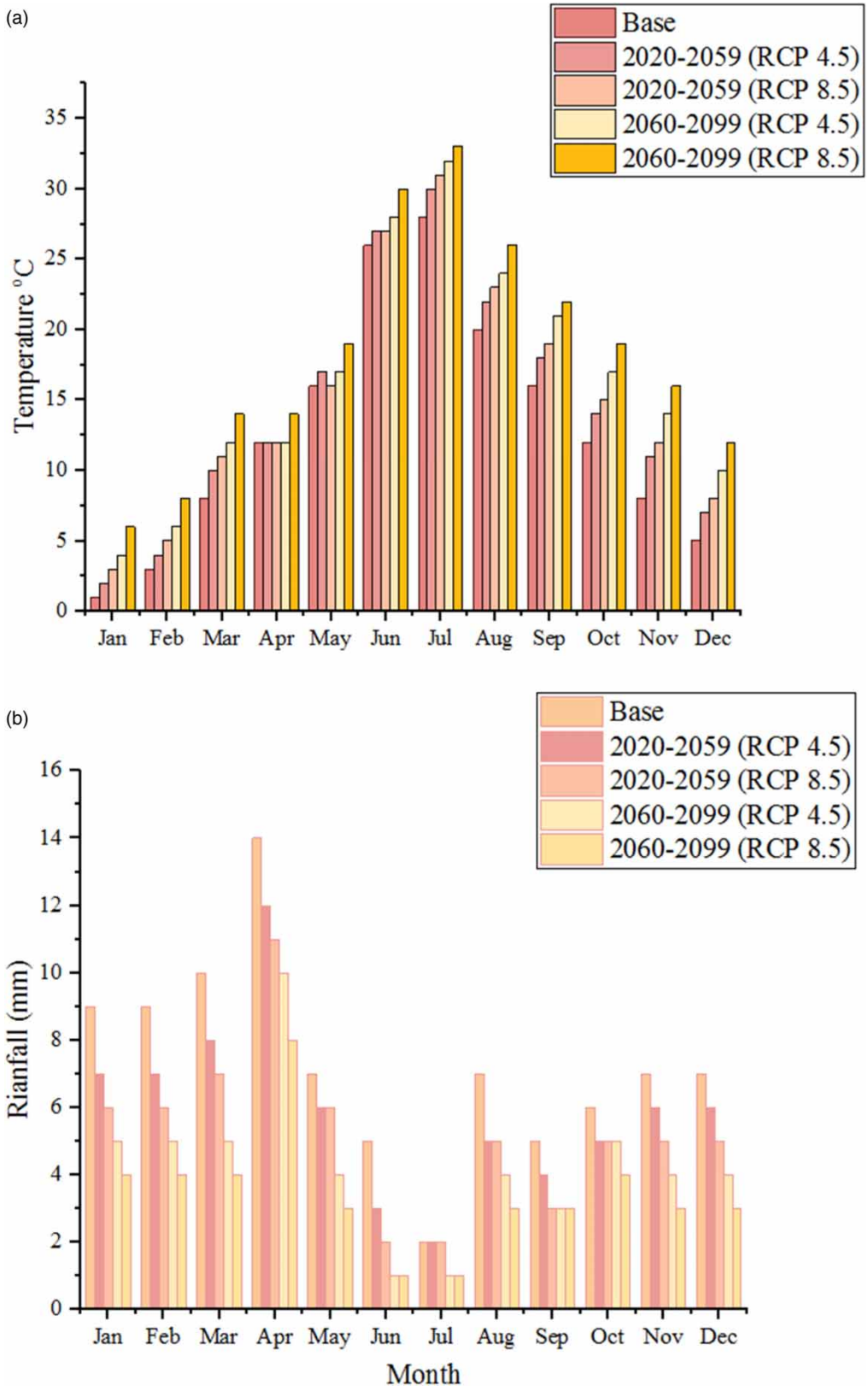

Figure 9 | Predicted rainfall (a) and temperature (b) for future short/medium- (2020–2059) and long-term (2060–2099) periods.

Table 1 | The top three best input combination of temperature and rainfall to predict GWL, based on GT test and associated Γ and V_{ratio} indices (TE, temperature; RA, rainfall)

Inputs	Γ	V_{ratio}
TE ($t-1$), RA ($t-1$), TE ($t-2$), RA ($t-3$), RA ($t-2$)	0.002	0.0008
TE ($t-1$), R ($t-1$), TE ($t-2$), RA ($t-3$), RA ($t-2$), TE ($t-3$)	0.005	0.0022
TE ($t-1$), R ($t-1$), TE ($t-2$), RA ($t-3$), RA ($t-2$), TE ($t-3$), TE (T − 4)	0.007	0.0031

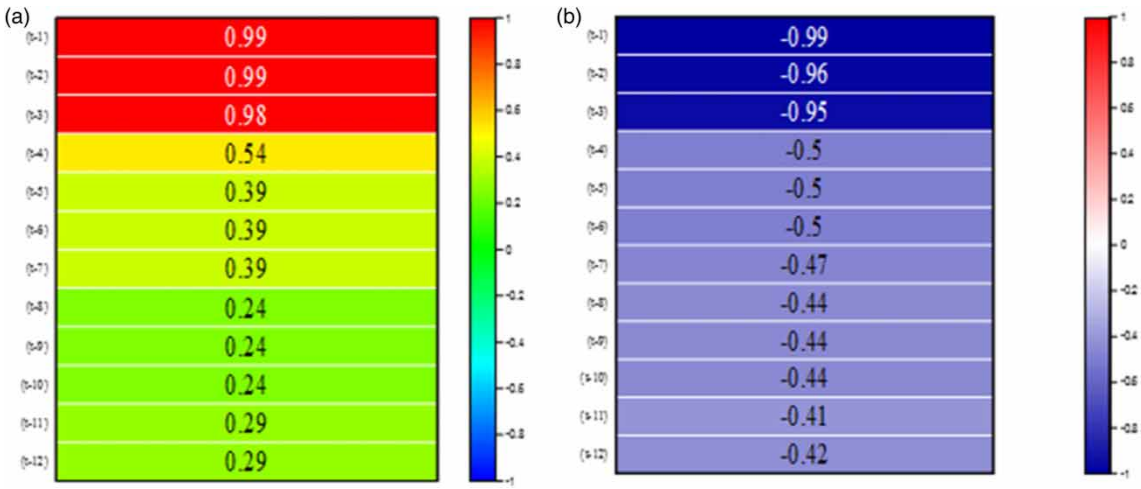

Figure 10 | Heat map correlation of (a) rainfall with GWL and (b) temperature and GWL.

lag time decreases the correlation value. Thus, the best input combination is chosen to predict GWL in both the base and future periods.

4.3. Sensitivity analysis to determine random parameters

In the structure of optimisation algorithms, random parameters play a key role in the modelling process. Thus, accurate determination of random parameters is an important task for modellers. In this study, a sensitivity analysis (SA) was undertaken to determine the values of random parameters. Population size (Pop) is an important parameter for optimisation algorithms. Figure 11(a) shows SA for determining the Pop of algorithms. The best value of Pop provides the lowest value of the objective function (RMSE). Pop = 100, Pop = 150, Pop = 200 and Pop = 20 are chosen for RSA, SSA, PSO, and GA, respectively, because they provide the lowest objective function. Figure 11(b) shows SA for determining the maximum number of iterations (IT). In SA, when a parameter value is changed, the values of other parameters are kept constant. IT = 100, IT = 150, IT = 150 and IT = 150 are chosen for RSA, SSA, PSO, and GA, respectively, because they provide the lowest objective function. Using a similar process, values of other random parameters are obtained. Values of other random parameters are shown in Table 2.

4.4. Investigation of the precision of models for predicting GWL

The accuracy of models for predicting GWL in the base period is investigated based on Figure 12. Figure 12(a) indicates the precision of models based on RMSE. RMSEs of IMM, ANN-RSA, ANN-SSA, ANN-PSO, ANN-GA, and ANN models are 2.12, 3.2, 4.58, 6.12, 6.98, and 7.89 m, respectively, in the testing level. Figure 12(b) indicates values of MAE for different models. IMM reduces the MAE of other models by 26–70%, respectively. Figure 12(c) compares the accuracy of models based on PBIAS. The IMM model reduces the PBIAS of hybrid and standalone models by 1–18%. Figure 12(d) shows values of NSE for different models. NSEs of IMM, ANN-RSA, ANN-SSA, ANN-PSO, ANN-GA, and ANN models are 0.96, 0.95, 0.90, 0.88, 0.84, and 0.76 respectively. The IMM model is the most accurate because it acts based on the outputs of multiple individual models. An IMM model is considered an ensemble model, which utilises the capability of all individual models to decrease the computational errors in the modelling process. RSA is a robust algorithm for tuning ANN parameters.

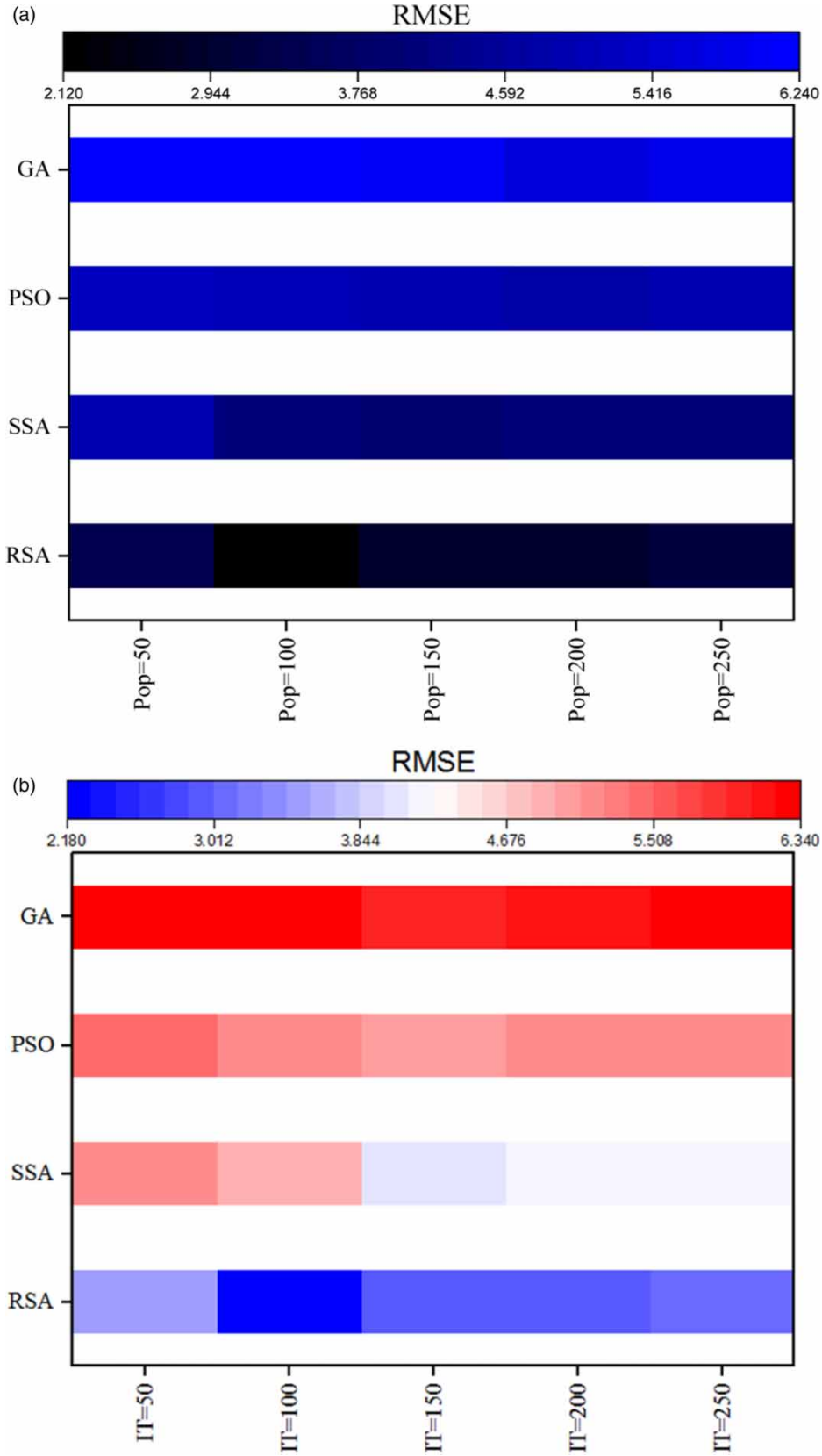

Figure 11 | Heat map of the SA of population size and number of iterations.

Table 2 | Values of random parameters

Algorithms
SSA, $\alpha_3 = 0.7$ and $\alpha_2 = 0.5$
PSO: $\nu_1 = \nu_2 = 2$ and ω: 0.70
GA: mutation probability: 0.6, crossover probability: 0.40

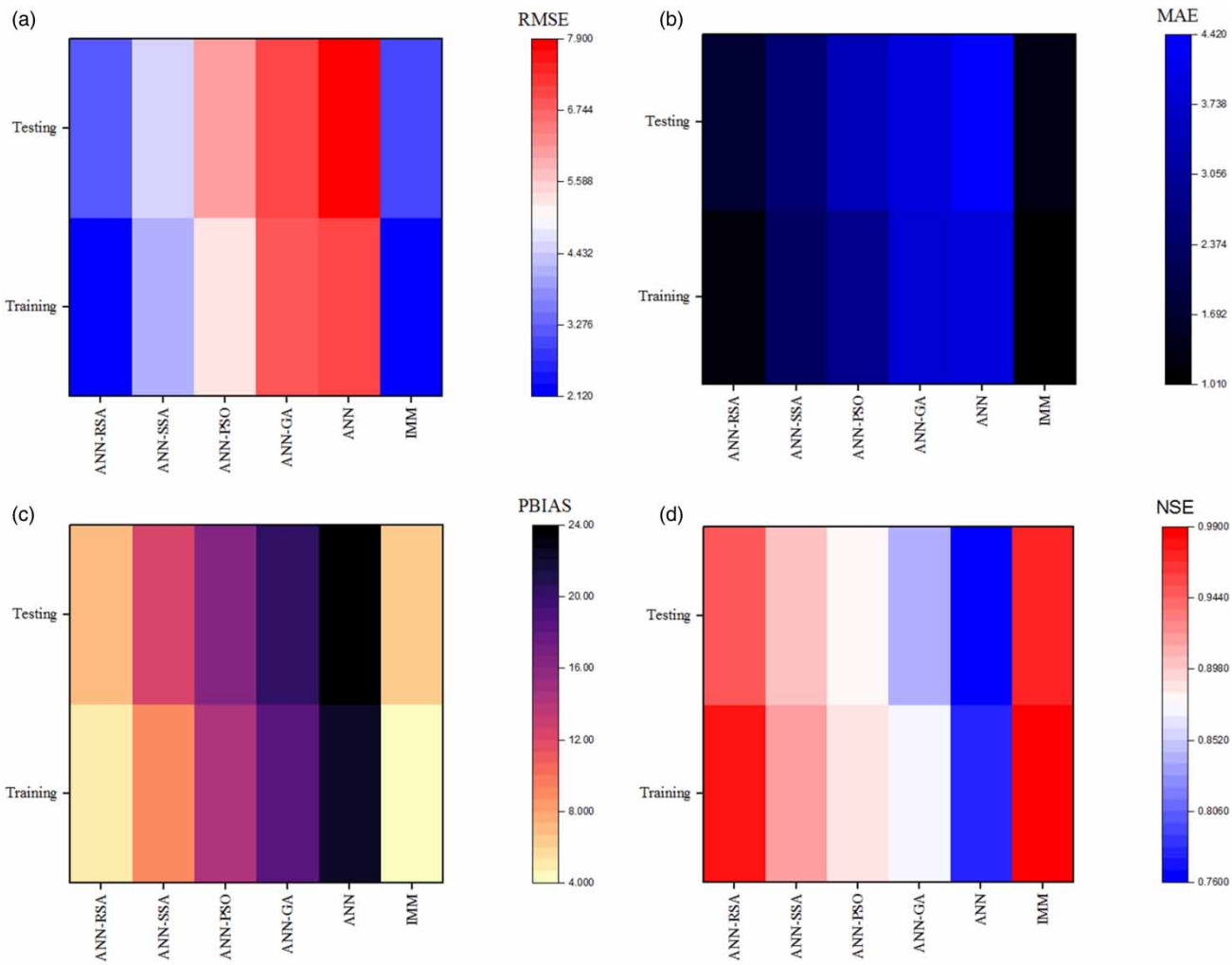

Figure 12 | Investigation of the accuracy of models based on (a) RMSE, (b) MAE, (c) PBIAS, and (d) NSE.

The use of fighting and chasing behaviours increases the potential of RSA for escape from local optima. Based on the results of this section, optimisation algorithms can effectively improve ANN models' performance. Consequently, choosing an optimisation algorithm that is robust and reliable is an important issue for modellers.

5. FURTHER DISCUSSION

5.1. Predicting GWL for future periods

In this study, the data for 312 months was used to avoid overfitting. As the best model, the IMM model is used to predict GWL for future periods using temperature and rainfall from RCP 4.5 and RCP 8.5 as inputs. The outputs of climate models are used

as inputs to IMM models in Section 4.1. Figure 13 indicates GWL for future periods. Monthly average GWLs for the base period of 1979–2005, the future period of 2020–2059 under RCP 4.5 and RCP 8.5, and the future period of 2060–2099 under RCP 4.5 and RCP 8.5 are 1,032.25, 1,031.21, 1,030.98, 1,030.32, and 1,030.11 m, respectively.

In the future, GWL variations will follow a similar pattern to the base period. GWL starts at a high level and ends at a low level. Variations caused by climate parameters in the future and the base period are the main causes of these variations. Global warming, increasing temperatures and decreasing rainfall are reasons for the decrease in GWL. Decision-makers will face a real challenge in relation to water supply in this basin. Decreasing GWL in the future may be detrimental to the economy and agriculture in the basin. The overexploitation of GWL in the current period has intensified water shortages in the future, as predicted for other areas worldwide. The use of renewable energy in the future could decrease water consumption for the generation of power. The status of GWL in the short, medium, and long-term shows that decision-makers should limit overexploitation of GW resources in the Yazd-Ardakan Plain basin. Furthermore, changes in cultivation patterns are an effective way of managing water resources in the basin. Figure 13 shows some peaks for GWL in the base and future periods. Wet durations and anomalous rainfall patterns may result in sudden fluctuations in GWL during study periods.

GW based on RCP 8.5 has the lowest level for the future period. To obtain a better understanding of variations in GWL for future periods under RCP 8.5, box plots of GWL for different months of the future period are plotted. Figure 14(a) shows GWL for 2020–2059 under RCP 8.5. As observed in this figure, the summer months experience the lowest GWL. The GWL for June and July ranges from 1,028.98 to 1,032.12 m. GWL for January varies from 1,030.98 to 1,034.78 m. The GWL for the winter and spring seasons is higher than for other seasons. In June and July, rainfall decreases and temperature increases significantly. Rainfall and temperature of July based on Figure 9(a) and 9(b) are 2 mm and 31 °C, respectively. Figure 14(b) shows GWL under RCP 8.5 for 2060–2099. The GWL for June and July ranges from 1,028.02 to 1,032.00 m. Regarding Figure 9(a) and 9(b), temperature and rainfall in July are 33 °C and 1 mm, respectively, for 2060–2099. Thus, increasing temperatures and decreasing rainfall will lead to a fall in GWL in the future. The box plots for the months of June and July for future periods indicate that the variation in GWL is high. Thus, water supply based on GW resources during the summer months in this basin faces high uncertainty and risk.

Figure 1A in Appendix A shows GWL depletion in the future under both investigated RCP scenarios. To compute GWL depletion, GWL for future periods is compared with that of the base period. As can be observed in Figure 1(a), GWL depletion in the basin in future periods of 2020–2059 under RCP 4.5, 2020–2059 under RCP 8.5, 2060–2099 under RCP 4.5, and 2060–2099 under RCP 8.5 is 0.60 to 0.88 m, 0.80 to 1.16 m, 1.49 to 1.97 m, and 1.75 to 1.98 m, respectively.

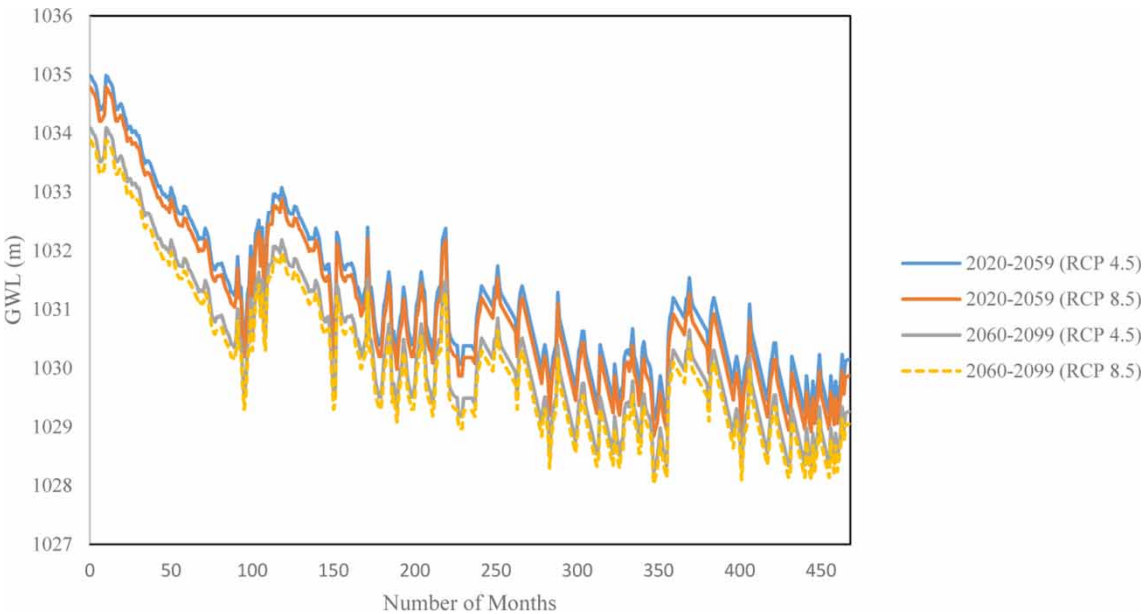

Figure 13 | GWL for future periods.

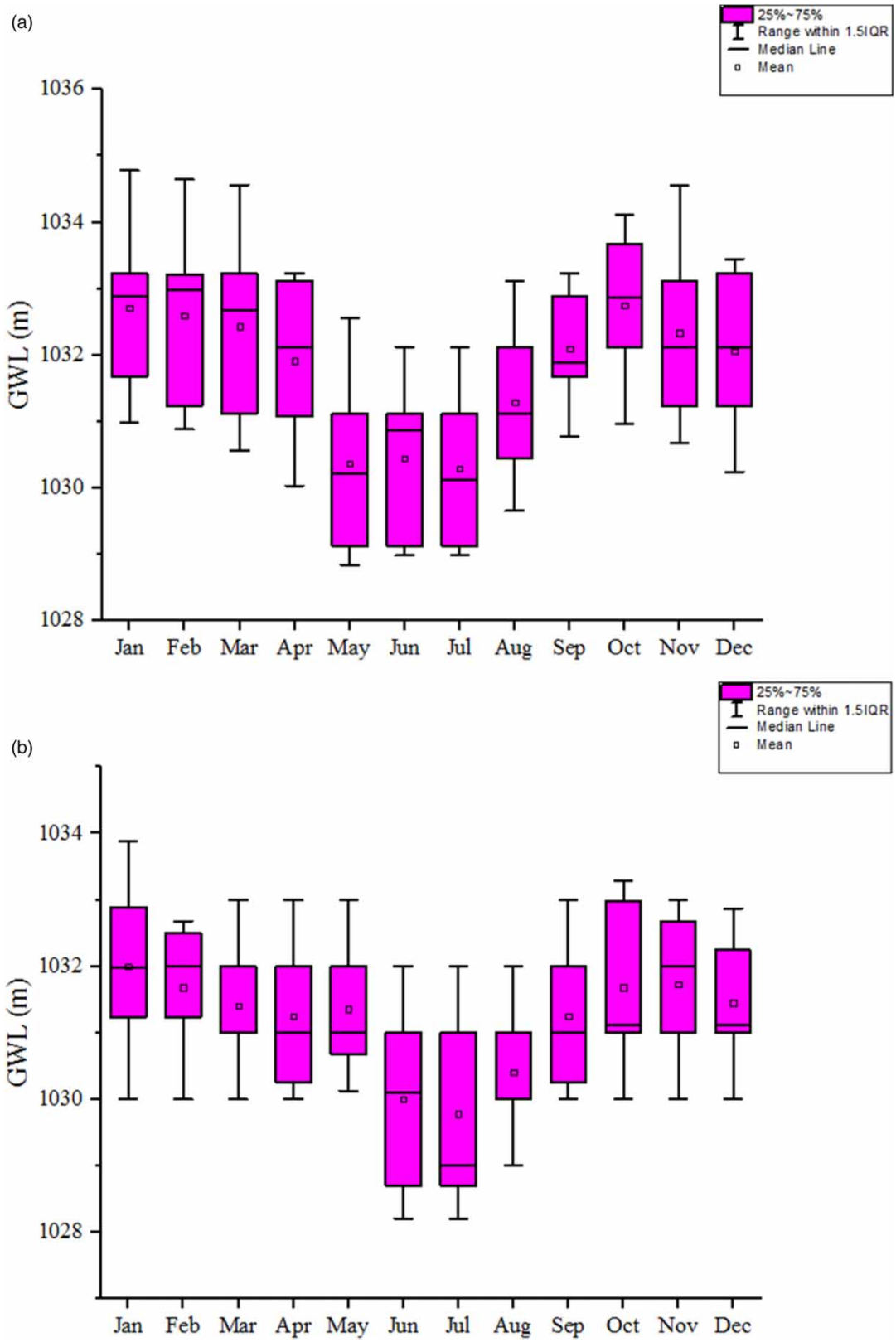

Figure 14 | Box plots of GWL for periods (a) 2020–2059 and (b) 2060–2099 based on RCP 8.5.

Thus, there is a fall in GWL in the future. Future studies can use other climate models such as CMIP6 for predicting temperature and rainfall in the future periods and compare GWL changes with those estimated in the current study.

However, results generally indicate that the status of GWL in future periods will decrease significantly. Thus, it is essential to suggest strategies for GW management based on the following points:

1. Desalination of water is an effective solution to decrease water consumption for agriculture and irrigation. Some greenhouses use solar radiation for freshwater production (Panahi *et al.* 2021). Desalinated water can be used to meet irrigation and agriculture demands. Water desalination can be a cheaper solution than water transformation plans for water supply (Ehteram *et al.* 2021b). Decision-makers suggested that water be transferred from the Persian Gulf (south of Iran) to Yazd, but it would be expensive.
2. The use of reclaimed water can be considered as an effective solution for the artificial recharge of aquifers (Sharafati *et al.* 2020b). Moreover, reclaimed water can be used for water supply in the agriculture sector. In this regard, a wastewater treatment plant can help with water treatment. Decision-makers might consider constructing ponds and transferring the treated municipal effluents into the ponds.
3. The installation of smart meters on the wells could be another effective solution for preventing overexploitation.
4. It is suggested to prevent the drilling of unauthorised wells by imposing strict rules.
5. Although agriculture is a source of income, encouraging people to use non-renewable energy for monetisation is another way to reduce GW consumption.
6. Raising public awareness and warning about the water crisis through the media is another solution.
7. The current study provides spatial and temporal maps of GWL for future and current periods. As a result, policymakers will have a deeper understanding of how GWL varies under climate change conditions. The current strategies would be ineffective for managing water resources in the future, and so policymakers can better design new strategies rooted in deeper knowledge of the local impacts of climate change. Nevertheless, implementing new policies is complex because they must satisfy all stakeholders. Based on the study's results, it may be recommended that cultivation patterns are changed to reduce irrigation requirements. In the current study, the GWL maps help decision-makers identify critical regions. Additionally, they can prepare new plans for agriculture and irrigation management in the basin based on the predicted rainfall, temperature, and GWL.
8. The study selected the ANN model because this model can be easily implemented. Also, the ANN parameters can be easily adjusted. Although there are models such as deep learning, these models have many unknown parameters. The authors explored convolutional neural networks and long short-term memory neural networks as robust deep learning tools for predicting GWL. However, the number of hidden layers, cell states, kernel functions, batch size, and number of epochs are unknown in the structure of the models. Thus, the implementation of these models may be complex. Also, this study used robust optimisers to develop the old version of ANN models.
9. Since the policymakers had defined the project based on the outputs of CMIP5 models, the modellers used these models in the current study. However, we suggested the CMPI6 models for predicting temperature and rainfall in future periods.

The current study had two main innovations: the IMM model and the hybrid GT. The GCM models were individual models, but the IMM improved the accuracy of the outputs by integrating the GCM outputs. Additionally, the hybrid test in the current study is a robust alternative to other feature available methods. Gamma tests automatically select the best inputs, while other methods, such as deep learning, require complex strategies. Additionally, the IMM model provides reliable results for GWL predictions. For predicting different variables, the IMM model is a robust ensemble method.

This study provides a deep understanding of the available water resources. Based on predicted GWL, decision-makers can plan for water supply in future periods. Moreover, the decreasing GWL of the future periods is a concern for decision-makers and policymakers. Water consumption can be reduced by changing the cultivation pattern. However, different suggestions for water supply have been presented by decision-makers. The water transfer plan from the Persian Gulf is one of the ideas for the water supply of the Yazd province. However, it should be considered that the water transfer plans are complex and have environmental effects.

The managed aquifer recharge (MAR) method for improving GW security is becoming increasingly popular worldwide (Ross & Hasnain 2018). The use of flood flows for irrigation and recharge, and the development of GW reserves in drought situations have been investigated and proposed by researchers. The use of conjunctive management and MAR to link surface water and GW is growing as a result of the development of sophisticated and creative methods. In this study, temporal and

spatial maps of GWL were provided by the models. These maps can support decision-makers in identifying the critical regions with the lowest GWL.

6. CONCLUSIONS

GWL prediction is important for water resource management in different basins. This research uses IMM and multiple hybrid ANN models to predict GWL in the Ardakan-Yazd Plain. Climate models are applied to predict temperature and rainfall in the short, medium, and long-term periods of 2020–2059 and 2060–2099, respectively. The monthly average rainfall for 2020–2059 under RCP 4.5 and RCP 8.5, and 2060–2099 under RCP 4.5 and RCP 8.5 is 5.91 mm, 4.25 mm, 5.25 mm, and 3.41 mm, respectively. Results reveal that the temperature in future periods will be higher than in the base period. The performance of models reveals that IMM models based on climate data enhance the precision of climate models for predicting these variables. The results reveal that the NSE of IMM and hybrid ANN models are very good (0.96 and 0.76–0.95, respectively). The investigation of GWL for the future and base periods indicates that GWL in the future is lower than that in the base period. GWL depletions for 2020–2059 under RCP 4.5 and RCP 8.5, and 2060–2099 under RCP 4.5 and RCP 8.5 are 0.60 to 0.88, 0.80 to 1.16, 1.49–1.97, and 1.75 to 1.98, respectively. This study can be developed using different models. In future studies, other methods such as machine-learning models can be applied for downscaling climate data. Besides, the potential of IMM can be benchmarked against other ensemble models.

AUTHOR CONTRIBUTIONS

Mohammad Ehteram, Zahra Kalntari, and Carla Sofia Ferreira conceptualised the work together; Kwok-Wing Chau applied formal techniques to analyse the data; Mohammad Ehteram, Zahra Kalntari, and Carla Sofia Ferreira involved in the design of methodology; Kwok-Wing Chau and Mohammad-Kazem Emami validated the data.

DATA AVAILABILITY STATEMENT

Data cannot be made publicly available; readers should contact the corresponding author for details.

CONFLICT OF INTEREST

The authors declare there is no conflict.

REFERENCES

Abbaszadeh, M., Ehteram, M., Ahmed, A. N., Singh, V. P. & Elshafie, A. 2021 The copper grade estimation of porphyry deposits using machine learning algorithms and Henry gas solubility optimization. *Earth Science Informatics*. https://doi.org/10.1007/s12145-021-00667-6.

Abdullah, S., Pradhan, R. C., Pradhan, D. & Mishra, S. 2021 Modeling and optimization of pectinase-assisted low-temperature extraction of cashew apple juice using artificial neural network coupled with genetic algorithm. *Food Chemistry*. https://doi.org/10.1016/j.foodchem.2020.127862.

Ashofteh, P.-S., Haddad, O. B., Akbari-Alashti, H. & Mariño, M. A. 2015Determination of irrigation allocation policy under climate change by genetic programming. *Journal of Irrigation and Drainage Engineering*. https://doi.org/10.1061/(asce)ir.1943-4774.0000807.

Banadkooki, F. B., Ehteram, M., Ahmed, A. N., Teo, F. Y., Fai, C. M., Afan, H. A. & El-Shafie, A. 2020 Enhancement of groundwater-level prediction using an integrated machine learning model optimized by whale algorithm. *Natural Resources Research* **29** (5), 3233–3252.

Chang, S. W., Nemec, K., Kalin, L. & Clement, T. P. 2016 Impacts of climate change and urbanization on groundwater resources in a barrier island. *Journal of Environmental Engineering* **142** (12), D4016001.

Chitsazan, M., Rahmani, G. & Neyamadpour, A. 2015 Forecasting groundwater level by artificial neural networks as an alternative approach to groundwater modeling. *Journal of the Geological Society of India*. https://doi.org/10.1007/s12594-015-0197-4.

Dhiman, G., Garg, M., Nagar, A., Kumar, V. & Dehghani, M. 2021 A novel algorithm for global optimization: rat swarm optimizer. *Journal of Ambient Intelligence and Humanized Computing*. https://doi.org/10.1007/s12652-020-02580-0.

Ehteram, M., Ferdowsi, A., Faramarzpour, M., Al-Janabi, A. M. S., Al-Ansari, N., Bokde, N. D. & Yaseen, Z. M. 2021a Hybridization of artificial intelligence models with nature inspired optimization algorithms for lake water level prediction and uncertainty analysis. *Alexandria Engineering Journal* **60** (2), 2193–2208.

Ehteram, M., Ahmed, A. N., Kumar, P., Sherif, M. & El-Shafie, A. 2021b Predicting freshwater production and energy consumption in a seawater greenhouse based on ensemble frameworks using optimized multi-layer perceptron. *Energy Reports***7**, 6308–6326.

Ehteram, M., Ahmed, A. N., Chow, M. F., Latif, S. D., Chau, K. W., Chong, K. L. & El-Shafie, A. 2022 Optimal operation of hydropower reservoirs under climate change. *Environment, Development and Sustainability* 1–33.

Farrokhi, A., Farzin, S. & Mousavi, S. F. 2021 Meteorological drought analysis in response to climate change conditions, based on combined four-dimensional vine copulas and data mining (VC-DM). *Journal of Hydrology* **603**, 127135.

Ghanbari-Adivi, E., Ehteram, M., Farrokhi, A. & Sheikh Khozani, Z. 2022 Combining radial basis function neural network models and inclusive multiple models for predicting suspended sediment loads. *Water Resources Management* 1–30.

Ghazi, B., Jeihouni, E. & Kalantari, Z. 2021 Predicting groundwater level fluctuations under climate change scenarios for Tasuj plain, Iran. *Arabian Journal of Geosciences*. https://doi.org/10.1007/s12517-021-06508-6.

Gong, Y., Zhang, Y., Lan, S. & Wang, H. 2016 A comparative study of artificial neural networks, support vector machines and adaptive neuro fuzzy inference system for forecasting groundwater levels near Lake Okeechobee, Florida. *Water Resources Management*. https://doi.org/10.1007/s11269-015-1167-8.

Gong, Y., Wang, Z., Xu, G. & Zhang, Z. 2018 A comparative study of groundwater level forecasting using data-driven models based on ensemble empirical mode decomposition. *Water (Switzerland)*. https://doi.org/10.3390/w10060730.

Hamidov, A., Khamidov, M. & Ishchanov, J. 2020 Impact of climate change on groundwater management in the northwestern part of Uzbekistan. *Agronomy*. https://doi.org/10.3390/agronomy10081173.

Huang, F., Huang, J., Jiang, S. H. & Zhou, C. 2017 Prediction of groundwater levels using evidence of chaos and support vector machine. *Journal of Hydroinformatics***19** (4), 586–606.

Jalali, S. M. J., Hedjam, R., Khosravi, A., Heidari, A. A., Mirjalili, S. & Nahavandi, S. 2020 Autonomous robot navigation using moth-flame-based neuroevolution. In: *Evolutionary Machine Learning Techniques* (S. Mirjalili, H. Faris & I. Aljarah, eds.). Springer, Singapore, pp. 67–83.

Lee, S., Lee, K. K. & Yoon, H. 2019 Using artificial neural network models for groundwater level forecasting and assessment of the relative impacts of influencing factors. *Hydrogeology Journal* **27** (2), 567–579.

Li, Y., Jia, M., Han, X. & Bai, X. S. 2021 Towards a comprehensive optimization of engine efficiency and emissions by coupling artificial neural network (ANN) with genetic algorithm (GA). *Energy*. https://doi.org/10.1016/j.energy.2021.120331.

Malik, A., Kumar, A., Kisi, O. & Shiri, J. 2019 Evaluating the performance of four different heuristic approaches with Gamma test for daily suspended sediment concentration modeling. *Environmental Science and Pollution Research*. https://doi.org/10.1007/s11356-019-05553-9.

Malik, A., Kumar, A., Kim, S., Kashani, M. H., Karimi, V., Sharafati, A., Ghorbani, M. A., Al-Ansari, N., Salih, S. Q., Yaseen, Z. M. & Chau, K. W. 2020 Modeling monthly pan evaporation process over the Indian central Himalayas: application of multiple learning artificial intelligence model. *Engineering Applications of Computational Fluid Mechanics*. https://doi.org/10.1080/19942060.2020.1715845.

Mirjalili, S., Gandomi, A. H., Mirjalili, S. Z., Saremi, S., Faris, H. & Mirjalili, S. M. 2017 Salpswarm algorithm: a bio-inspired optimizer for engineering design problems. *Advances in Engineering Software*. https://doi.org/10.1016/j.advengsoft.2017.07.002.

Mohanty, S., Jha, M. K., Raul, S. K., Panda, R. K. & Sudheer, K. P. 2015 Using artificial neural network approach for simultaneous forecasting of weekly groundwater levels at multiple sites. *Water Resources Management*. https://doi.org/10.1007/s11269-015-1132-6.

Natarajan, N. & Sudheer, C. 2020 Groundwater level forecasting using soft computing techniques. *Neural Computing and Applications* **32** (12), 7691–7708.

Noori, R., Karbassi, A. R., Moghaddamnia, A., Han, D., Zokaei-Ashtiani, M. H., Farokhnia, A. & Gousheh, M. G. 2011 Assessment of input variables determination on the SVM model performance using PCA, Gamma test, and forward selection techniques for monthly stream flow prediction. *Journal of Hydrology* **401** (3–4), 177–189.

Panahi, F., Ahmed, A. N., Singh, V. P., Ehtearm, M., elshafie, A. & Torabi Haghighi, A. 2021 Predicting freshwater production in seawater greenhouses using hybrid artificial neural network models. *Journal of Cleaner Production*. https://doi.org/10.1016/j.jclepro.2021.129721.

Patil, N. S., Chetan, N. L., Nataraja, M. & Suthar, S. 2020 Climate change scenarios and its effect on groundwater level in the Hiranyakeshi watershed. *Groundwater for Sustainable Development*. https://doi.org/10.1016/j.gsd.2019.100323.

Rezaie-balf, M., Naganna, S. R., Ghaemi, A. & Deka, P. C. 2017 Wavelet coupled MARS and M5 Model Tree approaches for groundwater level forecasting. *Journal of Hydrology*. https://doi.org/10.1016/j.jhydrol.2017.08.006.

Ross, A. & Hasnain, S. 2018 Factors affecting the cost of managed aquifer recharge (MAR) schemes. *Sustainable Water Resources Management* **4** (2), 179–190.

Seifi, A. & Riahi, H. 2020 Estimating daily reference evapotranspiration using hybrid gamma test-least square support vector machine, gamma test-ann, and gamma test-anfis models in an arid area of Iran. *Journal of Water and Climate Change*. https://doi.org/10.2166/wcc.2018.003.

Seifi, A., Ehteram, M., Soroush, F. & Haghighi, A. T. 2022 Multi-model ensemble prediction of pan evaporation based on the Copula Bayesian model averaging approach. *Engineering Applications of Artificial Intelligence* **114**, 105124.

Sharafati, A., Asadollah, S. B. H. S. & Neshat, A. 2020a A new artificial intelligence strategy for predicting the groundwater level over the Rafsanjan aquifer in Iran. *Journal of Hydrology*. https://doi.org/10.1016/j.jhydrol.2020.125468.

Sharafati, A., Asadollah, S. B. H. S. & Hosseinzadeh, M. 2020b The potential of new ensemble machine learning models for effluent quality parameters prediction and related uncertainty. *Process Safety and Environment Protection* https://doi.org/10.1016/j.psep.2020.04.045.

Shrestha, S., Bach, T. V. & Pandey, V. P. 2016 Climate change impacts on groundwater resources in Mekong Delta under representative concentration pathways (RCPs) scenarios. *Environmental Science and Policy*. https://doi.org/10.1016/j.envsci.2016.03.010.

Shrestha, S., Neupane, S., Mohanasundaram, S. & Pandey, V. P. 2020 Mapping groundwater resiliency under climate change scenarios: a case study of Kathmandu Valley, Nepal. *Environmental Research*. https://doi.org/10.1016/j.envres.2020.109149.

Singh, A., Malik, A., Kumar, A. & Kisi, O. 2018 Rainfall-runoff modeling in hilly watershed using heuristic approaches with gamma test. *Arabian Journal of Geosciences*. https://doi.org/10.1007/s12517-018-3614-3.

Tapoglou, E., Trichakis, I. C., Dokou, Z., Nikolos, I. K. & Karatzas, G. P. 2014 Groundwater-level forecasting under climate change scenarios using an artificial neural network trained with particle swarm optimization. *Hydrological Sciences Journal*. https://doi.org/10.1080/02626667.2013.838005.

Tigabu, T. B., Wagner, P. D., Hörmann, G., Kiesel, J. & Fohrer, N. 2021 Climate change impacts on the water and groundwater resources of the Lake Tana Basin, Ethiopia. *Journal of Water and Climate Change*. https://doi.org/10.2166/wcc.2020.126.

Yin, J., Medellín-Azuara, J., Escriva-Bou, A. & Liu, Z. 2021 Bayesian machine learning ensemble approach to quantify model uncertainty in predicting groundwater storage change. *Science of the Total Environment*. https://doi.org/10.1016/j.scitotenv.2020.144715.

Yoon, H., Hyun, Y., Ha, K., Lee, K. K. & Kim, G. B. 2016 A method to improve the stability and accuracy of ANN- and SVM-based time series models for long-term groundwater level predictions. *Computers and Geosciences*. https://doi.org/10.1016/j.cageo.2016.03.002.

Zhou, P., Wang, G. & Duan, R. 2020 Impacts of long-term climate change on the groundwater flow dynamics in a regional groundwater system: case modeling study in Alashan, China. *Journal of Hydrology*. https://doi.org/10.1016/j.jhydrol.2020.125557.

First received 19 May 2022; accepted in revised form 3 September 2022. Available online 15 September 2022